The FASEB Journal Express article fj.06-7061com. Published online December 21, 2006.

T-Cell inactivation and immunosuppressive activity induced by HIV gp41 via novel interacting motif

Itai Bloch,*[,1] Francisco J. Quintana,[†,1,2] Doron Gerber,*[,§] Tomer Cohen,* Irun R. Cohen,[†] and Yechiel Shai*[,3]

*Department of Biological Chemistry, and [†]Department of Immunology, the Weizmann Institute of Science, Rehovot, Israel

ABSTRACT **Fusion peptide (FP) of the HIV gp41 molecule inserts into the T cell membrane during virus-cell fusion. FP also blocks the TCR/CD3 interaction needed for antigen-triggered T cell activation. Here we used *in vitro* (fluorescence and immunoprecipitation), *in vivo* (T cell mediated autoimmune disease adjuvant arthritis), and *in silico* methods to identify the FP-TCR novel interaction motif: the α-helical transmembrane domain (TMD) of the TCR α chain, and the β-sheet 5–13 region of the 16 N-terminal aa of FP ($FP_{1–16}$). Deciphering the molecular mechanism of the immunosuppressive activity of FP provides a new potential target to overcome the immunosuppressant activity of HIV, and in addition a tool for down-regulating immune mediated inflammation.—Bloch, I., Quintana, F. J., Gerger, D., Cohen, T., Cohen, I. R., and Shai, Y. T-Cell inactivation and immunosuppressive activity induced by HIV gp41 via novel interacting motif.*FASEB J.* **21, 000–000 (2007)**

Key Words: membrane proteins · protein-membrane interaction · peptide-membrane interaction · transmembrane domain · recognition within membranes

ONE OF THE INITIAL STEPS in HIV infection is the fusion of the viral membrane with that of the target T cell membrane in a process catalyzed by HIV glycoprotein gp41 (1–3). Several regions in gp41 contribute to the fusion process; however, the 33 residues at the N terminus (the fusion peptide, $FP_{1–33}$) are of outstanding importance. Within $FP_{1–33}$, two different domains can be identified based on their biochemical characteristics and their role in membrane fusion. The N terminus of $FP_{1–33}$ contains a 16 aa-long hydrophobic stretch ($FP_{1–16}$), which inserts itself into the target membrane and is followed by a C-terminus hydrophilic region that lies parallel to the cell surface (4–6). Thus, during the process of membrane fusion, $FP_{1–16}$ anchors gp41 to the target membrane, and conformational changes in the three-dimensional structure of gp41 bring the membranes together and eventually complete the fusion process.

In addition to its fusogenic activity, $FP_{1–33}$ harbors immunosuppressive activities (7, 8). We have recently reported that FP can interact with the T cell receptor (TCR) and interfere with T cell activation (8). This activity of FP might function to suppress HIV-specific immunity and facilitate the spread of HIV to uninfected cells (8). Moreover, this immunosuppressive activity of FP might be exploited as an immunotherapeutic tool. Indeed, we have shown that FP can reduce the clinical signs of the experimental autoimmune T cell-mediated disease adjuvant arthritis (AA) (8).

The contribution of the different regions of FP to membrane fusion is well characterized; however, their role in the immunosuppressive activity of FP is still unknown. In this work, we identified the TCR/$FP_{1–33}$ interaction at the molecular level, providing a 3D model of the TCR/FP complex structure. A clear understanding of the molecular interactions mediating the immunosuppressive activity of FP will facilitate the evaluation of its contribution to HIV pathology and its exploitation as an immunotherapeutic tool.

MATERIALS AND METHODS

T cell proliferation assay

T cell proliferation assays were performed using popliteal and inguinal lymph node cells (LNC) removed 26 d after the injection of Mt in incomplete Freund's adjuvant (IFA), when strong T cell responses to PPD and Mt176–90 are detectable (9). Further details can be found in the supplementary materials.

Induction and assessment of adjuvant arthritis (AA)

AA was induced in groups of 6 rats by injecting 50 μl of Mt suspended in IFA (0.5 mg/ml) at the base of the tail, as previously reported (8). Further details can be found in the supplementary materials.

Fluorescent labeling of peptides

Resin-bound peptides were treated with 4-chloro-7-nitrobenz-2-oxa- 1,3-diazole fluoride [nitro benzoxadiazole (NBD)-F] or

[1] These authors contributed equally to this work.
[2] Current address: Center for Neurologic Diseases, Harvard Medical School, Boston, MA, USA.
[3] Correspondence: Department of Biological Chemistry, the Weizmann Institute of Science, Rehovot, 76100 Israel. E-mail: yechiel.shai@weizmann.ac.il
doi: 10.1096/fj.06-7061com

5-carboxytetramethylrhodamine, succinimidyl ester (Rho-SUC), respectively. The NBD-F and Rho-SUC fluorescent probes were purchased from Molecular Probes (Junction City, OR, USA). The reaction with NBD-F took place in DMF, and the reaction with Rhodamine in DMF containing 2% diisopropylethylamine as described previously (10). The fluorescent probes were used in an excess of two equivalents, leading to the formation of resin-bound N-terminal NBD or Rhodamine peptides. After 1 h, the resins were washed thoroughly with DMF and then with methylene chloride. The resin was dried under nitrogen flow and then cleaved for 3 h with TFA 95%, H_2O 2.5%, and triethylsilane 2.5%. The labeled peptides were cleaved as described above and purified on a RP-HPLC C4 column as described before (8). Unless stated otherwise, stock solutions of concentrated peptides were maintained in DMSO to avoid aggregation of the peptides prior to use. The final concentration of DMSO in each experiment (5% v/v) had no effect on the system.

Colocalization of peptides with membrane molecules

A2b cells that had been activated for 72 h with PPD and APC were fixed with 4% paraformaldehyde for 15 min on ice and washed with PBS. In control experiments resting A2b cells (8–10 d after a previous activation by APC incubated with antigen) were used. A2b cells activated with PPD were also investigated without fixation with 4% paraformaldehyde. The cells were then treated with 2% BSA in PBS at room temperature to block unspecific binding. After 30 min the cells were divided into aliquots containing 50,000 cells per 100 μl and either αTCR-FITC or αCD4-FITC was added (1:100) for 2 h. The Rho-labeled FP fragments were added during the last 5 min of incubation at a final concentration of 0.5–1μM. The cells were then washed with PBS and deposited onto a glass slide. The labeled cell samples were observed under a fluorescence confocal microscope. FITC excitation was set at 488 nm, with the laser set at 20% power to minimize bleaching of the fluorophore. Fluorescence was recorded from 505–525 nm. Rhodamine excitation was set at 543 nm, with the laser set at 5% power. Fluorescence data were collected from 560 nm and up.

Coimmunoprecipitation of fluorescence-labeled peptides with TCR molecules

Activated A2b T cells (2×10^6) were cultured for 1 h at 37°C in the presence of FP fragments (25 μg/ml), or medium alone, and lysed for 15 min on ice in 0.1 ml lysis buffer (11). Insoluble material was removed by centrifugation at 10,000 g for 10 min at 4°C. The lysate was then incubated overnight with Protein A-plus Agarose beads (Santa Cruz Biotechnology, Inc., Santa Cruz, CA, USA) bound to antibodies to the rat TCR, CD28, actin, HSP60 or MHC class I (data shown only for TCR and MHC class I). The antibodies reactive against the rat TCR (clone R73) or HSP60 (clone LK1) were purified from the respective hybridomas at our lab; antibodies to rat CD28, actin and the rat MHC class I were purchased from Serotec (Oxford, UK). After an overnight incubation at 4°C, the beads were washed with lysis buffer and boiled for 10 min, and the protein supernatant run in a 16% SDS-PAGE. The presence of coimmunoprecipitated peptide was detected by the Typhoon 9400 variable mode imager.

Fluorescence resonance energy transfer (FRET) measurements

NBD-labeled peptides served as donors in the FRET measurements to the acceptor Rho-labeled peptides. Prior to the measurements lipid mixture of PC:SM:Cho (1:1:1 w/w/w ratio) was prepared in $CHCL_3$:MeOH (2:1 v/v ratio), this lipid mixture was then dissolved in PBS buffer filtered by miniextruder reaching filter pore size of 0.1 μm to obtain large unilamellar vesicles (LUVs). The NBD-Labeled crude protein (CP) was introduced into the LUV and fluorescence spectra were read (Aminco Bowman series 2 luminescence spectrometer) in the presence or absence of Rho-labeled FP fragments. In FRET competition experiments, after the addition of both donor and acceptor peptides to the system, an unlabeled competing peptide was added and the fluorescence intensity was measured before and after this addition. In all fluorescence experiments involving FP fragments, we used peptide/lipid ratio of $\sim8\times10^{-5}$ to ensure that FP concentration is kept below the fusogenic concentration according to the former reported value of $\sim5\times10^{-3}$ (12). In this peptide/lipid ratio, the peptide fragments reside inside the membrane. Energy transfer efficiency (E) was determined experimentally from the ratio between the fluorescence intensity of the donor molecules in the presence (I_{da}) and in the absence (I_d) of acceptor molecules at the wavelength of the maximal donor's emission. The percentage of energy-transfer efficiency E (%) is given by:

$$E(\%) = (1-I_{da}/I_d)\times100.$$

The contribution of the buffer and the vesicles was subtracted from all spectra prior to the calculations. To eliminate the contribution to the total fluorescence signal of the acceptors direct excitation, the acceptors fluorescence was also subtracted.

Statistical significance

The InStat 2.01 program (Graph Pad Software, San Diego, CA, USA) was used for statistical analysis. The Student's *t* test and the Mann-Whitney *U* test were conducted to assay significant differences between the different experimental groups. Further details on the experimental methods including the entire simulation procedure are given in the Supplemental Data.

RESULTS

Inhibition of T cell activation *in vitro*

The CD3/TCR complex is stabilized by electrostatic interactions established between the transmembrane domains (TMD) of the CD3 and different TCR subunits. We have previously shown that FP_{1-33} associates with the TCR and interferes with the CD3/TCR crosstalk (8). Since FP_{1-16} is known to insert itself into the T cell membrane to trigger membrane fusion, we investigated whether FP_{1-16} could also interact with the TCR and interfere with T cell activation. We, therefore, synthesized a set of peptides spanning the whole hydrophobic N terminus (FP_{1-16}) or parts of it (FP_{1-8} and FP_{9-16}) and studied their ability to interfere with antigen-triggered T cell proliferation (**Table 1**). Primed LNC were taken from Mt immunized rats 26 d after immunization, when they show a strong proliferative response to the immunodominant mycobacterial antigens PPD and Mt176–90 (9, 13). FP_{1-16} and FP_{1-33} displayed similar inhibitory effects when tested at a

TABLE 1. *Peptide designations and sequences*

Designation	Start	Sequence[a]	End	Protein
$FP_{1–33}$	512	AVGIGALFLGFLGAAGSTMGARSMTLTVQARQL	544	gp41
$FP_{1–16}$	512	AVGIGALFLGFLGAAG	527	gp41
$FP_{1–8}$	512	AVGIGALF	519	gp41
$FP_{9–16}$	520	LGFLGAAG	527	gp41
$FP_{5–13}$	516	LFLGFLG	524	gp41
CP	–	GLRILLLKV	–	Rat TCRα
2G CP	–	GLGILLLGV	–	Rat TCRα
TCRα TMD	251	VMGLRILLLKVAGFNLLMTL	270	Rat TCRα
F9L	125	LREEMRIQLNDMNSALTTAIPLFA	148	Cry1Ac
Mt 176–190	176	EESNTFGLQLELTEG	190	Mt HSP65

[a]Underlined amino acids stand for mutation in the original sequence.

concentration of 25 μg/ml (**Fig. 1**). However, at lower concentrations, $FP_{1–16}$ was less active than was $FP_{1–33}$ (Fig. 1). No inhibition of T cell proliferation was observed when the T cells where incubated with $FP_{1–8}$ or $FP_{9–16}$. Thus, the inhibitory effects of $FP_{1–33}$ on T cell activation *in vitro* can be recapitulated to some degree by its N-terminal hydrophobic region, contained in $FP_{1–16}$.

Inhibition of T cell activation *in vivo*

Adjuvant arthritis (AA) is a T cell-mediated experimental autoimmune disease inducible in Lewis rats by immunization with Mt in oil. We have previously shown that $FP_{1–33}$ can interfere with T cell activation *in vivo* and ameliorate the course of AA (8). To analyze the effect that $FP_{1–16}$ might have on T cell activation *in vivo*, we studied its effects on the progression of AA. $FP_{1–16}$ administration at the time of AA induction led to a significant decrease in the signs of AA, both in terms of clinical AA score (**Fig. 2*A***) and leg swelling (Fig. 2*B*). Note that the *in vivo* immunomodulatory activity of $FP_{1–16}$ was equal to that produced by a similar amount of $FP_{1–33}$. No amelioration was seen when we used a PBS control group (Fig. 2*A* and *B*) or a control peptide (data not shown and (8).

The activity of the T cells that mediate AA can be followed *in vivo* by studying the DTH response to Mt

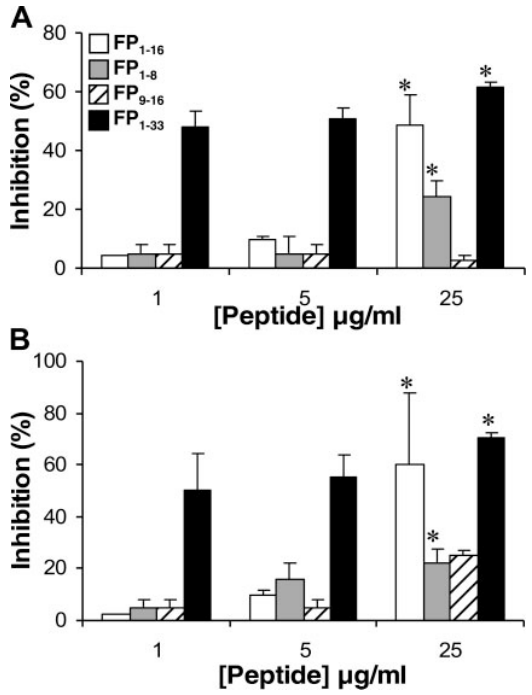

Figure 1. Inhibition of T cell proliferation by FP fragments. LNC from Mt immunized rats were activated *in vitro* with PPD (*A*) or the Mt176–90 peptide (*B*) in the presence of $FP_{1–16}$, $FP_{1–8}$, $FP_{9–16}$, or $FP_{1–33}$ and the proliferative responses were assayed. Similar results were obtained in at least three additional experiments. $*P < 0.05$ compared to $FP_{9–16}$ treated cells.

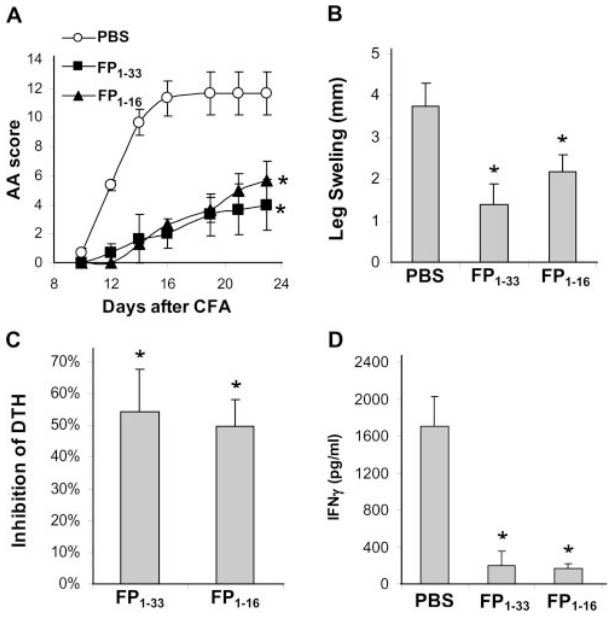

Figure 2. $FP_{1–16}$ inhibits AA. AA was induced by immunization to Mt in oil, mixed with PBS, FP1–16, or FP1–33. Arthritis was scored every two or three days starting at day 10 (*A*); the leg swelling was measured at day 26 (*B*); the DTH response to PPD was measured at day 16 (*C*); and IFNγ secretion was measured at day 26 on stimulation of LNC with HSP71 or Mt176–90 and normalized to values obtained for PBS group (*D*). $*P < 0.05$ compared to the PBS group.

(14). The administration of $FP_{1–16}$ led to a decrease of ~50% in the Mt-specific DTH response, similar to that observed in $FP_{1–33}$-treated AA rats (Fig. 2*C*). Treatment with the shorter peptides or PBS did not affect the DTH response.

The T cells that mediate AA are characterized by the secretion of IFNγ on activation with PPD or mt176–90 *ex vivo*. Accordingly, treatments that ameliorate AA, such as administration of $FP_{1–33}$, are usually associated with a decreased INF-γ secretion by LNC on stimulation with mycobacterial antigens. The administration of the $FP_{1–16}$ peptide led to a significant ($P<0.01$) decrease in the secretion of IFNγ by the LNC of AA rats on stimulation with Mt antigens, comparable with that seen in $FP_{1–33}$-treated rats (Fig. 2*D*). All in all, these results indicate that $FP_{1–16}$ inhibits T cell activation both *in vitro* and *in vivo*.

Colocalization of $FP_{1–16}$ with the TCR in the membrane of activated T cells

To better understand the molecular interactions mediating the inhibition of T cell activation by $FP_{1–16}$, we studied the distribution of rhodamine-conjugated $FP_{1–16}$, $FP_{1–8}$ and $FP_{9–16}$ in the membrane of activated rat A2b T cells. **Figure 3** shows that $FP_{1–16}$ colocalized with the TCR, while $FP_{1–8}$ and $FP_{9–16}$ showed largely a cytoplasmatic distribution. Thus, $FP_{1–16}$ reproduced the pattern of colocalization with the TCR observed for $FP_{1–33}$ (8).

$FP_{1–16}$ physically interacts with the TCR

We have shown that $FP_{1–33}$ can be immunoprecipitated with anti-TCR antibodies, suggesting the formation of a TCR/$FP_{1–33}$ complex in the membrane of activated T cells. To map the region in $FP_{1–33}$ that mediates this interaction, we tested the ability of Rho-labeled $FP_{1–16}$, $FP_{1–8}$ and $FP_{9–16}$ to coimmunoprecipitate with TCR molecules, or with MHC-I as a control. Rho-labeled

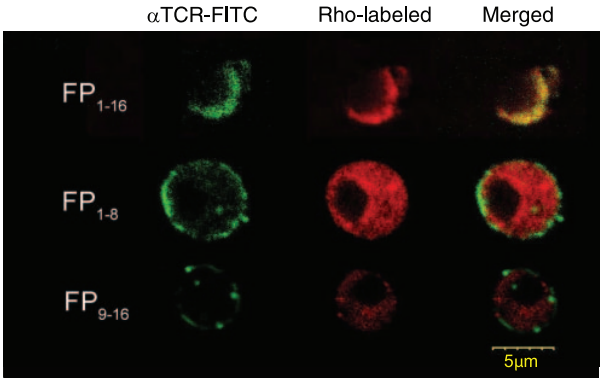

Figure 3. $FP_{1–16}$ colocalizes with the TCR receptor. $FP_{1–16}$, $FP_{1–8}$ and $FP_{9–16}$ were conjugated to rhodamine (Rho) and used to study peptide binding to the membranes of activated T cells, in combination with FITC-labeled antibodies to the TCR.

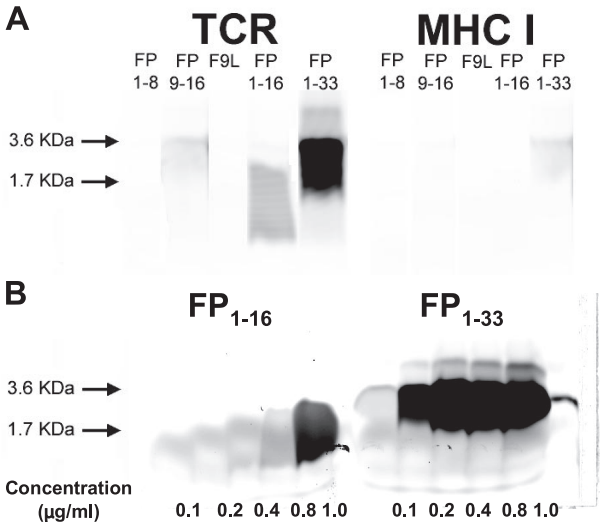

Figure 4. $FP_{1–16}$ interacts with the TCR with a lower affinity than $FP_{1–33}$. *A)* A2b T cells were incubated with 1 μM Rho-labeled $FP_{1–16}$, $FP_{1–8}$, $FP_{9–16}$, $FP_{1–33}$, or F9L for 1 h, lysed, and immunoprecipitated with antibodies to TCR or MHC class I. Bound protein were separated by SDS-PAGE and analyzed for the presence of the fluorescence-labeled peptides. *B)* A2b T cells were incubated with different amounts of Rho-labeled $FP_{1–16}$ or $FP_{1–33}$ for 1 h, lysed, and immunoprecipitated with antibodies to TCR or MHC class I. Bound proteins were separated by SDS-PAGE and analyzed for the presence of the fluorescence-labeled peptides.

$FP_{1–33}$ and $FP_{1–16}$ could be coprecipitated with TCR molecules, although the interaction seemed to be weaker for $FP_{1–16}$; no coimmunoprecipitation was seen when we used the control peptide Rho-F9L or a control antibody (Ab) to MHC-I (**Fig. 4*A***). We compared the affinity of the TCR/$FP_{1–33}$ and the TCR/$FP_{1–16}$ interactions by performing a series of coprecipitation experiments using different concentrations of Rho-labeled $FP_{1–16}$ or $FP_{1–33}$. Figure 4*B* shows that, although both $FP_{1–16}$ and $FP_{1–33}$ can be coprecipitated with the TCR receptor, the interaction mediated by $FP_{1–33}$ seems to be of higher affinity: lower concentrations of $FP_{1–33}$ were needed to detect a significant coprecipitation with TCR molecules (Fig. 4*B*). Thus, the 16 N terminus aa of $FP_{1–33}$, $FP_{1–16}$, can account for much of the TCR/$FP_{1–33}$ interaction.

Interaction between $FP_{1–16}$ and TCRα TMD within the TCR complex

The coimmunoprecipitation results showed in Fig. 4 suggested a physical interaction between $FP_{1–16}$ and the TCR, but did not identify the target sequence recognized within the TCR complex. However, the hydrophobic nature of $FP_{1–16}$ suggested that it interacts with components of the TCR located within the membrane, such as the transmembrane domain (TMD) of the TCR. To study the potential interaction of the TCR TMD with $FP_{1–16}$, we competed the coimmunoprecipitation of $FP_{1–16}$ and TCR molecules with a peptide

representing the TMD of the TCR α chain (TCRα) (termed CP) or a mutated CP peptide (2G CP) (Table 1). 2G CP is a mutant peptide derived from CP, where the two charged aa known to mediate the interaction with CD3 subunits (15, 16) have been substituted by glycines. Competition with unlabeled CP (in a 4× molar excess) led to a significant decrease in the amount of Rho-labeled $FP_{1–33}$ coimmunoprecipitated (**Fig. 5*A***). However, no decrease was observed when the coimmunoprecipitation reaction included an excess of the control peptide 2G CP. These results suggest that $FP_{1–16}$ targets the TCRα TMD in an interaction that involves the two positive charges of the TCRα TMD.

We also studied the interaction between $FP_{1–33}$ and the TCRα TMD by following fluorescence resonance energy transfer (FRET) between NBD-labeled CP and Rho-labeled $FP_{1–33}$ synthetic peptides in lipid vesicles composed of PC:SM:Cho (1:1:1 w/w/w ratio). When a 4-fold molar excess of unlabeled CP was added to lipid membranes containing NBD-labeled CP and Rho-labeled $FP_{1–33}$, a significant decrease ($P<0.01$) in the FRET signal was detected (Fig. 5*B*). No change was detected on the addition of 2G CP (Fig. 5*B*). These results suggest a direct interaction between the TCRα TMD and FP within the T cell membrane.

Molecular dynamics simulation: equilibration properties

To confirm and visualize our experimental results, we conducted a 30 ns molecular dynamics simulation with an explicit atom description. We used the sequence of the $FP_{1–16}$ with the sequence of the TCRα peptide extended by the three additional C-terminal aa AGF. A model of the complex between $FP_{1–16}$ and TCRα CP was created and positioned in a fully hydrated DMPC bilayer (**Fig. 6*A***). We used DMPC bilayers in the MD simulation because of the following criteria: *i)* DMPC bilayers have been intensively studied both experimentally and theoretically, which allows us to validate the correctness of the simulation parameters by comparing measurable entities (*e.g.*, electronic density, lipid order parameter S_{CD}, bilayer thickness, etc.) of the membrane to those of previous studies; *ii)* the use of DMPC bilayers in the simulation allows us to maintain the most biologically relevant bilayer phase (L_α phase) in the biologically relevant temperature (310°K); *iii)* in the simulation conducted in this study we used an atomistic detailed membrane model rather than an implicit model of membrane. The use of DMPC lipids preserves the global parameters required for describing a model membrane, and furthermore allows careful examina-

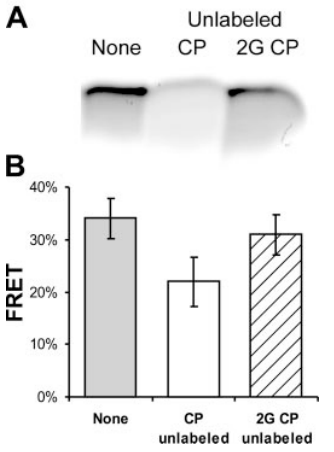

Figure 5. $FP_{1–33}$ targets the TCRα TMD. *A)* Activated A2b T cells were incubated with Rho-labeled $FP_{1–33}$ with no additives (none) or in the presence of a unlabeled peptide coding for the wild-type (WT) TCRα TMD (CP) or of a mutant TCRα TMD in which the 2 positive residues have been replaced by glycines (2G CP). After 1 h, the cells were lysed and immunoprecipitated with antibodies to TCR. Bound protein were separated by SDS-PAGE and analyzed for the presence of the fluorescence-labeled peptides. *B)* NBD-labeled CP (0.1 μM) and Rho-labeled $FP_{1–33}$ (0.05 μM) were dissolved in lipid vesicles that contained no other peptides, or that contained 4× unlabeled CP or CP 2G and the FRET between the two peptides was recorded. Data is presented as percent of FRET

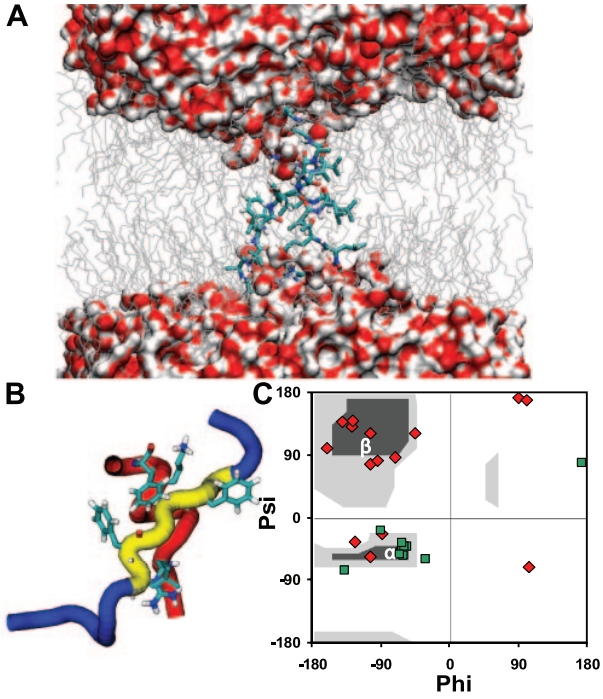

Figure 6. Analysis of the $FP_{1–16}$-TCRα interaction within a membrane bilayer using a 30 ns molecular dynamics simulation. *A)* Representative snapshot of the simulation system at equilibrium: *i*) Water molecules in surface representation colored by atoms, *ii*) Peptides with dynamic bond representation colored by atoms, and *iii*) DMPC molecules as gray lines. *B)* The peptide complex backbone is shown as tubes to emphasize the orientation and structure of the complex inside the membrane. The TCRα chain is colored in red, $FP_{1–16}$ in blue and residues 6–11, which comprise the interacting segment within the $FP_{1–16}$, highlighted in yellow. The important Phe, Arg, and Lys residues are shown in detail. *C)* A Ramachandran plot of the average C_α dihedral angles, throughout the equilibrium state, shows $FP_{1–16}$ values in red diamonds and the TCRα values in green squares.

tion of the specific lipid-peptide interactions; *iv)* the DMPC membrane model does capture several important natural membrane properties as it is zwitterionic and it creates a hydrophobic layer. The evolution of the total energy, density, and box volume of the system during the 30 ns simulation was primarily used for determining whether the system had reached equilibrium (simulation profiles are presented in Supplemental Fig. 1*A–C*). A decrease in the simulation box volume was observed during the first 300 ps restrained run and in the first 5 ns of the full unrestrained run, which enabled the system to reach a pressure of 1 bar. The simulation box volume decreased from 254.06 nm^3 to the final equilibrium volume of 227.68 nm^3. Based on these parameters, equilibrium was achieved after ~12 ns. Thus, we considered the last 15 ns of the simulation to be in equilibrium. Statistical and structural analysis was made on the basis of data taken from the equilibrated phase only.

A root mean square deviation (RMSD) profile showed that the peptide structure reached stability after ~4.5 ns of the unrestrained run. Supplemental Fig. 1*D* shows the averaged RMSD profile of the complex and the separate RMSD for both TCRα CP and $FP_{1–16}$. These results indicate that the CP is much more stable and in fact keeps its helical structure throughout the simulation while the FP looses its initial conformation rapidly and adopts a β-strand. This latter conformation remained stable for the rest of the simulation.

Molecular dynamics simulation: general bilayer properties

To estimate the validity of a simulation, one should compare the obtained system parameters with that of the relevant experimental system. Such a comparison can be made with experiments done on fluid, fully hydrated lipid bilayers, which are the most biologically relevant (L_α phase) to such systems. The methods used for detection of bilayer parameters vary from volumetric measurements to optical methods such as diffuse X-ray scattering, liquid crystallographic X-ray and Neutron diffraction measurements (17, 18). The density profile of the simulation box along the bilayer surface normal (the *z*-axis of the simulation box) shows typical bilayer properties with no water penetration into the lipid environment while the peptide complex remains inside the bilayer (Supplemental Fig. 2*A*). The average area per lipid headgroup is 62Å (2); this is in agreement with the determined experimental value (19–21). Bilayer thickness (D_{pp}), which is the average distance between lipid headgroups at each monolayer, is 35Å (obtained from the electron density profiles of the bilayer) and is close to the experimental value of 36Å (17) for a pure hydrated DMPC bilayer. The microscopic structure of lipid molecules and the ordering of acyl chains are characterized through the deuterium order parameter S_{CD}. The deuterium order parameter measures the orientational order of the lipid tails. It can be computed for each carbon atom in the lipid acyl chains by averaging over all equivalent atoms in all DMPC. Although slightly lower, as expected by the perturbation of the peptides used, S_{CD} values, which are shown in Supplemental Fig. 2*B*, are comparable with recent published results from a DMPC bilayer simulation (22).

The β-sheet folded $FP_{1–16}$ interacts with the α-helical TMD of the TCRα

We found that the potential interface between the two peptides in the complex is stable throughout the production run. The structural data show that the largest contribution to complex stability was made by residues GALFLGFLG, in the 5–13 region of $FP_{1–16}$, which interacts with the TCRα TMD (Fig. 6*A* and *B*). In the TCRα TMD, the Arg and Lys residues were found in the interpeptide interface contributing the most to the stability of the complex (Fig. 6*B*). Interestingly, these observations are in agreement with our experimental results, showing the need of the Arg and Lys aa to compete with the coimmunoprecipitation of $FP_{1–33}$ and the TCR (Fig. 5). As it seems from the equilibrium phase of the complex, the two charged residues interact with the polar atoms of the FP backbone to stabilize the interaction, mainly through hydrogen bonds. However, as both Arg and Lys have long and bulky side chains, they are in close contact to the FP residues. Specifically, Arg of the TCRα TMD interacts with the two N terminus Leu of the FP, and Lys of the TCRα TMD interacts with the C-terminus Leu and Ala of the FP. In addition, during the equilibrium phase of the simulation (last 15 ns) the FP N terminus Phe shifts from one rotameric state to another. Only in the second rotameric state, the TCRα TMD Phe interacts with the FP Phe. This shift occurs at ~25 ns and remains stable until the end of the simulation. Therefore, we can conclude that it does not play a crucial role in the initial formation of the complex. However, this interaction contributes to the complex stability by expanding the contact surface between the two peptides. Energetically, there is no significant change in the overall energy profile of the complex interaction energy, probably due to compensation by other elements within the complex.

Remarkably, analysis of the $FP_{1–16}$ C_α dihedral angles demonstrated a shift from the initial α-helical structure into a β-strand, as shown in the Ramachandran plot in Fig. 6*C*. The TCR α chain kept its helical structure throughout the entire simulation (Fig. 6*C*). Thus, the molecular dynamics simulation suggests a direct interaction between residues 6 to 12 of the β-sheet folded FP and the α-helical TMD of the TCR α-chain.

$FP_{5–13}$ inhibits T cell activation

Our molecular dynamics simulation suggested that the 5–13 region in FP mediated the interaction between FP and the TCRα TMD (Fig. 6). To confirm this finding experimentally, we synthesized a peptide corresponding to the 5–13 region of $FP_{1–16}$ (GALFLGFLG, named

$FP_{5–13}$) and studied its ability to interfere with T cell activation. We have described previously that FP inhibits the activation of the A2b T cell line by its cognate peptide Mt176–90 (8); this inhibition results from the activity of FP on A2b T cells, and not on the APC presenting Mt176–90 (8). To study the effect of $FP_{5–13}$ on T cell activation, A2b cells were incubated with increasing concentrations of $FP_{5–13}$ and stimulated with the Mt176–90 and irradiated APC. **Figure 7** shows that addition of $FP_{5–13}$ led to a dose-dependant inhibition of T cell proliferation; this effect was statistically significant ($P<0.005$) when compared to the effect of the control peptide p277. Hence, the interaction between FP and the TCRα TMD is mediated by the 5–13 region of $FP_{1–16}$.

DISCUSSION

In this work we analyzed the inhibition of T cell activation by FP at a molecular level. Our results show that the TCRα TMD is targeted by $FP_{1–16}$, which interferes with the antigen-triggered activation of T cells *in vivo* and *in vitro*. The molecular dynamic simulations pinpointed the interaction to the 5–13 region of $FP_{1–16}$. Indeed, we found that $FP_{5–13}$ interferes with the antigen-triggered activation of T cells *in vitro*.

The insertion of FP into the membrane of the target cells anchors the molecular machinery that promotes HIV membrane fusion (23–25). Recent data indicate that this event takes place at the interface of the APC/T cell interaction, leading to the invasion of the T cell via the immune synapse (26–28). The immune synapse is an organized array of receptors and signaling molecules responsible for T cell activation on recognition of the agonist T cell epitope displayed on the surface of the APC. Thus, the localization of the immunosuppressive motif in $FP_{1–16}$ suggests that the APC/T cell physical interaction is exploited by the virus to simultaneously invade the T cell and interfere with T cell activation. Taken together with the fact that HIV preferentially infects HIV specific T cells (29–32), our observations might explain the unsolved puzzle of decreased HIV-specific T cell immunity amid general T cell hyperactivation observed in HIV-infected patients in the early stages of the infection (33, 34). Other immunosuppressive activities described for HIV might collaborate in the takeover of the immune response that finally leads to the collapse of the host's immune system (25, 35).

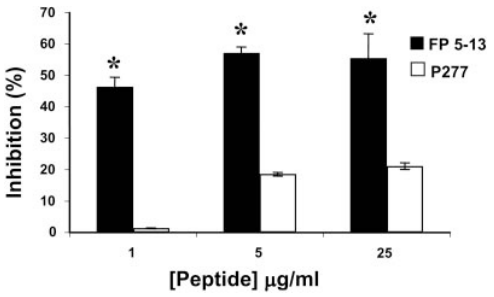

Figure 7. $FP_{5–13}$ inhibits T cell proliferation. A2b T cells were activated with the Mt176–90 peptide and APC in the presence of $FP_{5–13}$ or p277 and the proliferative responses were assayed. Similar results were obtained in at least three additional experiments. * $P < 0.005$ compared to p277-treated cells.

Obviously, FP plays a central role in viral replication; the virus cannot replicate unless it infects a cell. Viral proteins are under the constant pressure of the host's immune system, which they escape by the generation of mutant variants. However some viral peptides, like FP, cannot accommodate a large degree of variability without compromising their functionality. Indeed, FP is one of the most conserved sequences within the viral genome, and HIV strains harboring a mutant FP show a decreased ability to infect target cells and replicate *in vivo* (36). In this context, the colocalization of the fusogenic and the immunosuppressor activities in FP might diminish the immunogenicity of FP, protecting it from the immune system's pressure. This hypothesis is supported by the increased immunogenicity found in FP mutants that harbor a decreased immunosuppressive activity (8).

In this work we identified the cellular target of FP experimentally. Similarly to what we previously described for $FP_{1–33}$ (8), $FP_{1–16}$ colocalizes with the TCR in the T cell membrane (Fig. 3). Indeed, FRET studies suggested that $FP_{1–16}$ implants within 50 Å of the TCR (data not shown). Moreover, $FP_{1–16}$ could be coprecipitated with the TCR from the T cell membrane (Fig. 4). Thus, the signals required for guiding the colocalization of $FP_{1–16}$ to the membrane and the interaction with the TCR are included in the first 16 N-terminal aa contained in $FP_{1–16}$. Using two different experimental systems, a competitive immunoprecipitation assay and FRET (Fig. 5*A,B*), we could conclude that FP directly interacts with the TMD of the TCR α-chain. This interaction is mediated by the two positively charged aa in the TCRα TMD (arginine and lysine); their removal led to a significant decrease in the interaction with FP. The participation of the arginine and lysine residues of the TCRα TMD in the interaction with the FP is further supported by the results of the molecular dynamics simulation (Fig. 6) and by the inhibition exerted by $FP_{5–13}$ (Fig. 7).

Analysis of the experimental data and the computer simulation highlighted two outstanding features of the TCR/FP interaction: 1) it is a specific interaction between a β-sheet (the FP) and an α-helix (the CP); 2) FP interacts with polar aa in the target TCRα TMD, although FP itself is not charged. Although unusual, such interactions might be favored by the special features of intermolecular interactions within the membrane milieu (37, 38).

The FP manifests structural diversity; it has been shown to adopt both α-helical and β-sheet conformations (39–49). However, a ^{13}C FTIR structural model of

FP within the 70 N-terminal aa of gp41 shows that FP is likely to adopt a β-sheet conformation in the context of the ectodomain (50). The results of the molecular dynamics simulation showed an unusual conformational transition of the $FP_{1–16}$ peptide from an α-helix into a β-strand during the simulation trajectory. This conformational change allowed the creation of hydrogen bonds between the TCRα polar residues and the FP backbone's carbonyl atoms that further stabilized the FP/TCRα complex inside the membrane. Thus, our model suggests that polar residues on the TCRα TMD contribute to the stabilization of transmembrane complexes by interacting with the backbone of $FP_{1–16}$. This observation is in agreement with the results depicted in Fig. 5: the FP/TCR interaction is diminished when the two polar aa in the TCRα TMD are substituted with glycines.

Nevertheless, our model does not completely satisfy the energetic requirements of the hydrogen donor/acceptor atoms of the backbone between an α-helix and a single β-strand inside the membrane. Note, however, that the gp41 protein forms trimers (51) on the viral membrane and that FP itself oligomerizes in solution (44, 50); this would allow the FP to adopt a β-sheet conformation and still satisfy the energy requirement for hydrogen bonds that would stabilize its interaction with the α-helix TCRα TMD. The formation of FP trimers could not be accounted for in our model because of the need to reduce the complexity of the system while focusing primarily on the FP/TCRα interaction. To our knowledge, this molecular dynamics model is the first prediction of such a complex transmembrane structure.

The targeting of the TCR/CD3 interaction by FP is reminiscent of the use of the CP peptide as an immunomodulator to inhibit T cell activation (52) and interfere with the progression of autoimmune arthritis and diabetes (52, 53). Notably the interaction of CP with the TCR/CD3 complex is also dictated by some unexpected structural constraints (53). Our results suggest that HIV might have naturally evolved a strategy to interfer with the TCR/CD3 interaction as a way to thwart a specific immune response to gp41. Overall, deciphering the molecular mechanism of the immunosuppressive activity of FP provides a new potential target to overcome the immunosuppressant activity of HIV, and in addition a tool for down-regulating immune-mediated disorders. FJ

We thank Vladimir Kiss for his help with the confocal microscopy and Batya Zarmi for her help with peptide purification. Y.S. has the Harold S. and Harriet B. Brady Professorial Chair in Cancer Research, and I.R.C. is the Mauerberger Professor of Immunology at the Weizmann Institute of Science, the Director of the Center for the Study of Emerging Diseases, Jerusalem, and the Director of the National Center for Biotechnology in the Negev, at the Ben-Gurion University of the Negev. D.G.'s research was supported by the Hughes and Sheila Potiker Postdoctoral Fellowship in Autoimmune Disease Research. This study was supported in part to Y.S. by the Israel Science Foundation and by a grant from the Estate of Julius and Hanna Rosen.

REFERENCES

1. Kliger, Y., Peisajovich, S. G., Blumenthal, R., and Shai, Y. (2000) Membrane-induced conformational change during the activation of HIV-1 gp41. *J. Mol. Biol.* **301,** 905–914
2. Sackett, K., and Shai, Y. (2002) The HIV-1 gp41 N-terminal heptad repeat plays an essential role in membrane fusion. *Biochemistry* **41,** 4678–4685
3. Wexler-Cohen, Y., Sackett, K., and Shai, Y. (2005) The role of the N-terminal heptad repeat of HIV-1 in the actual lipid mixing step as revealed by its substitution with distant coiled coils. *Biochemistry* **44,** 5853–5861
4. Peisajovich, S. G., Epand, R. F., Pritsker, M., Shai, Y., and Epand, R. M. (2000) The polar region consecutive to the HIV fusion peptide participates in membrane fusion. *Biochemistry* **39,** 1826–1833
5. Peisajovich, S. G., and Shai, Y. (2003) Viral fusion proteins: multiple regions contribute to membrane fusion. *Biochim. Biophys. Acta* **1614,** 122–129
6. Epand, R. M. (2003) Fusion peptides and the mechanism of viral fusion. *Biochim. Biophys. Acta* **1614,** 116–121
7. Haynes, B. F., Arthur, L. O., Frost, P., Matthews, T. J., Langlois, A. J., Palker, T. J., Hart, M. K., Scearce, R. M., Jones, D. M., McDanal, C., *et al.* (1993) Conversion of an immunogenic human immunodeficiency virus (HIV) envelope synthetic peptide to a tolerogen in chimpanzees by the fusogenic domain of HIV gp41 envelope protein. *J. Exp. Med.* **177,** 717–727
8. Quintana, F. J., Gerber, D., Kent, S. C., Cohen, I. R., and Shai, Y. (2005) HIV-1 fusion peptide targets the TCR and inhibits antigen-specific T cell activation. *J. Clin. Invest.* **115,** 2149–2158
9. Quintana, F. J., Carmi, P., Mor, F., and Cohen, I. R. (2002) Inhibition of adjuvant arthritis by a DNA vaccine encoding human heat shock protein 60. *J. Immunol.* **169,** 3422–3428
10. Gerber, D., and Shai, Y. (2000) Insertion and organization within membranes of the delta-endotoxin pore-forming domain, helix 4-loop-helix 5, and inhibition of its activity by a mutant helix 4 peptide. *J. Biol. Chem.* **275,** 23602–23607
11. Adachi, T., Schamel, W. W., Kim, K. M., Watanabe, T., Becker, B., Nielsen, P. J., and Reth, M. (1996) The specificity of association of the IgD molecule with the accessory proteins BAP31/BAP29 lies in the IgD transmembrane sequence. *EMBO J.* **15,** 1534–1541
12. Agirre, A., Flach, C., Goni, F. M., Mendelsohn, R., Valpuesta, J. M., Wu, F., and Nieva, J. L. (2000) Interactions of the HIV-1 fusion peptide with large unilamellar vesicles and monolayers. A cryo-TEM and spectroscopic study. *Biochim. Biophys. Acta* **1467,** 153–164
13. Quintana, F. J., Carmi, P., Mor, F., and Cohen, I. R. (2003) DNA fragments of the human 60-kDa heat shock protein (HSP60) vaccinate against adjuvant arthritis: identification of a regulatory HSP60 peptide. *J. Immunol.* **171,** 3533–3541
14. Van Eden, W., Holoshitz, J., Nevo, Z., Frenkel, A., Klajman, A., and Cohen, I. R. (1985) Arthritis induced by a T-lymphocyte clone that responds to Mycobacterium tuberculosis and to cartilage proteoglycans. *Proc. Natl. Acad. Sci. U. S. A.* **82,** 5117–5120
15. Call, M. E., Pyrdol, J., Wiedmann, M., and Wucherpfennig, K. W. (2002) The organizing principle in the formation of the T cell receptor-CD3 complex. *Cell* **111,** 967–979
16. Call, M. E., Pyrdol, J., and Wucherpfennig, K. W. (2004) Stoichiometry of the T-cell receptor-CD3 complex and key intermediates assembled in the endoplasmic reticulum. *EMBO J.* **23,** 2348–2357
17. Nagle, J. F., and Tristram-Nagle, S. (2000) Structure of lipid bilayers. *Biochim. Biophys. Acta* **1469,** 159–195
18. Nagle, J. F., and Tristram-Nagle, S. (2000) Lipid bilayer structure. *Curr. Opin. Struct. Biol.* **10,** 474–480
19. Petrache, H. I., Tristram-Nagle, S., and Nagle, J. F. (1998) Fluid phase structure of EPC and DMPC bilayers. *Chem. Phys. Lipids* **95,** 83–94
20. Petrache, H. I., Dodd, S. W., and Brown, M. F. (2000) Area per lipid and acyl length distributions in fluid phosphatidylcholines determined by (2)H NMR spectroscopy. *Biophys. J.* **79,** 3172–3192
21. Kucerka, N., Liu, Y., Chu, N., Petrache, H. I., Tristram-Nagle, S., and Nagle, J. F. (2005) Structure of fully hydrated fluid phase

DMPC and DLPC lipid bilayers using X-ray scattering from oriented multilamellar arrays and from unilamellar vesicles. *Biophys. J.* **88,** 2626–2637
22. Gorfe, A. A., Pellarin, R., and Caflisch, A. (2004) Membrane localization and flexibility of a lipidated ras peptide studied by molecular dynamics simulations. *J. Am. Chem. Soc.* **126,** 15277–15286
23. Lawless, M. K., Barney, S., Guthrie, K. I., Bucy, T. B., Petteway, S. R., Jr., and Merutka, G. (1996) HIV-1 membrane fusion mechanism: structural studies of the interactions between biologically-active peptides from gp41. *Biochemistry* **35,** 13697–13708
24. Peisajovich, S. G., and Shai, Y. (2002) New insights into the mechanism of virus-induced membrane fusion. *Trends. Biochem. Sci.* **27,** 183–190
25. Johnson, W. E., and Desrosiers, R. C. (2002) Viral persistance: HIV's strategies of immune system evasion. *Annu. Rev. Med.* **53,** 499–518
26. Garcia, E., Pion, M., Pelchen-Matthews, A., Collinson, L., Arrighi, J. F., Blot, G., Leuba, F., Escola, J. M., Demaurex, N., Marsh, M., and Piguet, V. (2005) HIV-1 trafficking to the dendritic cell-T-cell infectious synapse uses a pathway of tetraspanin sorting to the immunological synapse. *Traffic* **6,** 488–501
27. McDonald, D., Wu, L., Bohks, S. M., KewalRamani, V. N., Unutmaz, D., and Hope, T. J. (2003) Recruitment of HIV and its receptors to dendritic cell-T cell junctions. *Science* **300,** 1295–1297
28. Van Kooyk, Y., and Geijtenbeek, T. B. (2003) DC-SIGN: escape mechanism for pathogens. *Nat. Rev. Immunol.* **3,** 697–709
29. Pope, M., Betjes, M. G., Romani, N., Hirmand, H., Cameron, P. U., Hoffman, L., Gezelter, S., Schuler, G., and Steinman, R. M. (1994) Conjugates of dendritic cells and memory T lymphocytes from skin facilitate productive infection with HIV-1. *Cell* **78,** 389–398
30. Kwon, D. S., Gregorio, G., Bitton, N., Hendrickson, W. A., and Littman, D. R. (2002) DC-SIGN-mediated internalization of HIV is required for trans-enhancement of T cell infection. *Immunity* **16,** 135–144
31. Geijtenbeek, T. B., Kwon, D. S., Torensma, R., van Vliet, S. J., van Duijnhoven, G. C., Middel, J., Cornelissen, I. L., Nottet, H. S., KewalRamani, V. N., Littman, D. R., *et al.* (2000) DC-SIGN, a dendritic cell-specific HIV-1-binding protein that enhances trans-infection of T cells. *Cell* **100,** 587–597
32. Sugaya, M., Lore, K., Koup, R. A., Douek, D. C., and Blauvelt, A. (2004) HIV-infected Langerhans cells preferentially transmit virus to proliferating autologous CD4+ memory T cells located within Langerhans cell-T cell clusters. *J. Immunol.* **172,** 2219–2224
33. Woods, T. C., Roberts, B. D., Butera, S. T., and Folks, T. M. (1997) Loss of inducible virus in CD45RA naive cells after human immunodeficiency virus-1 entry accounts for preferential viral replication in CD45RO memory cells. *Blood* **89,** 1635–1641
34. Douek, D. C., Brenchley, J. M., Betts, M. R., Ambrozak, D. R., Hill, B. J., Okamoto, Y., Casazza, J. P., Kuruppu, J., Kunstman, K., Wolinsky, S., *et al.* (2002) HIV preferentially infects HIV-specific CD4+ T cells. *Nature* **417,** 95–98
35. Douek, D. C., Picker, L. J., and Koup, R. A. (2003) T cell dynamics in HIV-1 infection. *Annu. Rev. Immunol.* **21,** 265–304
36. Freed, E. O., Myers, D. J., and Risser, R. (1990) Characterization of the fusion domain of the human immunodeficiency virus type 1 envelope glycoprotein gp41. *Proc. Natl. Acad. Sci. U. S. A.* **87,** 4650–4654
37. Senes, A., Ubarretxena-Belandia, I., and Engelman, D. M. (2001) The Calpha —H. O hydrogen bond: a determinant of stability and specificity in transmembrane helix interactions. *Proc. Natl. Acad. Sci. U. S. A.* **98,** 9056–9061
38. Fleming, K. G., and Engelman, D. M. (2001) Specificity in transmembrane helix-helix interactions can define a hierarchy of stability for sequence variants. *Proc. Natl. Acad. Sci. U. S. A.* **98,** 14340–14344
39. Yang, J., Parkanzky, P. D., Khunte, B. A., Canlas, C. G., Yang, R., Gabrys, C. M., and Weliky, D. P. (2001) Solid state NMR measurements of conformation and conformational distributions in the membrane-bound HIV-1 fusion peptide. *J. Mol. Graph Model* **19,** 129–135
40. Yang, J., Gabrys, C. M., and Weliky, D. P. (2001) Solid-state nuclear magnetic resonance evidence for an extended beta strand conformation of the membrane-bound HIV-1 fusion peptide. *Biochemistry* **40,** 8126–8137
41. Slepushkin, V. A., Andreev, S. M., Sidorova, M. V., Melikyan, G. B., Grigoriev, V. B., Chumakov, V. M., Grinfeldt, A. E., Manukyan, R. A., and Karamov, E. V. (1992) Investigation of human immunodeficiency virus fusion peptides. Analysis of interrelations between their structure and function. *AIDS Res. Hum. Retroviruses* **8,** 9–18
42. Rafalski, M., Lear, J. D., and DeGrado, W. F. (1990) Phospholipid interactions of synthetic peptides representing the N-terminus of HIV gp41. *Biochemistry* **29,** 7917–7922
43. Mobley, P. W., Waring, A. J., Sherman, M. A., and Gordon, L. M. (1999) Membrane interactions of the synthetic N-terminal peptide of HIV-1 gp41 and its structural analogs. *Biochim. Biophys. Acta* **1418,** 1–18
44. Kliger, Y., Aharoni, A., Rapaport, D., Jones, P., Blumenthal, R., and Shai, Y. (1997) Fusion peptides derived from the HIV type 1 glycoprotein 41 associate within phospholipid membranes and inhibit cell-cell Fusion. Structure- function study. *J. Biol. Chem.* **272,** 13496–13505
45. Gordon, L. M., Curtain, C. C., Zhong, Y. C., Kirkpatrick, A., Mobley, P. W., and Waring, A. J. (1992) The amino-terminal peptide of HIV-1 glycoprotein 41 interacts with human erythrocyte membranes: peptide conformation, orientation and aggregation. *Biochim. Biophys. Acta* **1139,** 257–274
46. Chang, D. K., Cheng, S. F., and Chien, W. J. (1997) The amino-terminal fusion domain peptide of human immunodeficiency virus type 1 gp41 inserts into the sodium dodecyl sulfate micelle primarily as a helix with a conserved glycine at the micelle-water interface. *J. Virol.* **71,** 6593–6602
47. Chang, D. K., Chien, W. J., and Cheng, S. F. (1997) The FLG motif in the N-terminal region of glucoprotein 41 of human immunodeficiency virus type 1 adopts a type-I beta turn in aqueous solution and serves as the initiation site for helix formation. *Eur. J. Biochem.* **247,** 896–905
48. Gordon, L. M., Mobley, P. W., Pilpa, R., Sherman, M. A., and Waring, A. J. (2002) Conformational mapping of the N-terminal peptide of HIV-1 gp41 in membrane environments using (13)C-enhanced Fourier transform infrared spectroscopy. *Biochim. Biophys. Acta* **1559,** 96–120
49. Gordon, L. M., Mobley, P. W., Lee, W., Eskandari, S., Kaznessis, Y. N., Sherman, M. A., and Waring, A. J. (2004) Conformational mapping of the N-terminal peptide of HIV-1 gp41 in lipid detergent and aqueous environments using 13C-enhanced Fourier transform infrared spectroscopy. *Protein Sci.* **13,** 1012–1030
50. Sackett, K., and Shai, Y. (2005) The HIV fusion peptide adopts intermolecular parallel beta-sheet structure in membranes when stabilized by the adjacent N-terminal heptad repeat: a 13C FTIR study. *J. Mol. Biol.* **350,** 790–805
51. Center, R. J., Leapman, R. D., Lebowitz, J., Arthur, L. O., Earl, P. L., and Moss, B. (2002) Oligomeric structure of the human immunodeficiency virus type 1 envelope protein on the virion surface. *J. Virol.* **76,** 7863–7867
52. Manolios, N., Collier, S., Taylor, J., Pollard, J., Harrison, L. C., and Bender, V. (1997) T-cell antigen receptor transmembrane peptides modulate T-cell function and T cell-mediated disease. *Nat. Med.* **3,** 84–88
53. Gerber, D., Quintana, F. J., Bloch, I., Cohen, I. R., and Shai, Y. (2005) D-enantiomer peptide of the TCR alpha transmembrane domain inhibits T-cell activation in vitro and in vivo. *FASEB J.* **19,** 1190–1192

Received for publication August 9, 2006.
Accepted for publication September 22, 2006.